 doi:10.20944/preprints201809.0280.v1

Fine-Resolution Mapping of Fine Dust Concentration in Urban Areas and Population Exposure Analysis via Dispersion Modeling

Seungwoo Son [1], Dongwoo Kim [1], Hyungjin Jeon [1,*], Youngeun Kang [2], Seogcheol Kim [3], Kyunghak Cho [3] and Jaejin Yu [1,*]

[1] Department of Land and Water Environment Research, Korea Environment Institute, Sejong 30147, Korea; swson@kei.re.kr (S.S.); dwkim@kei.re.kr (D.K.)
[2] Research Department, Site Planning Co., Ltd, Busan 48505, Korea; jiyoon8936@gmail.com
[3] Boolt Simulation, Inc, Seoul 06664, Korea; sckim@boolt.co.kr (S.K.); kyunghak@boolt.co.kr (K.C.)
* Correspondence: hjjeon@kei.re.kr (H.J.); jjyu@kei.re.kr (J.Y.)

Abstract: It is currently difficult to obtain accurate fine dust information in residential areas due to the insufficient number of air quality monitoring systems and spatial imbalances. Therefore, a detailed particulate matter dispersion model including factors such as land use and meteorological information was developed in this study and used to create fine dust concentration distribution maps. The fine dust concentration distribution maps currently available to citizens were compared with those obtained by dispersion modeling, and population distribution data were employed to compare the populations exposed to fine dust according to the two methods. The results of the existing method and the developed particulate matter dispersion model differed significantly. For instance, the PM2.5 concentrations in Daejeon, South Korea, on February 17, 2018, were 56% "Good" and 44% "Moderate," according to the existing method, while they were 31% "Good," 26% "Moderate," 28% "Unhealthy," and 15% "Very Unhealthy," according to the dispersion model. Furthermore, the existing method indicated that no portion of the population was exposed to poor fine dust concentrations, while the proposed model revealed that over 170 thousand people were exposed to such concentrations. These results on fine dust distributions will contribute to sustainable urban and environmental planning.

Keywords: Atmospheric pollution; dispersion modeling; particulate matter; urban and environmental planning

1. Introduction

Atmospheric pollution is a major environmental issue that has critical impacts on society, the economy, and human health [1–3]. Especially in urban areas, various atmospheric pollutants are generated in increasing amounts due to various types of land use and human activity. The severity of atmospheric pollutants is also growing in South Korea due to the development and revitalization of urban areas, and public interest in this matter is rising based on the increasing examples of the impacts of atmospheric pollution on health.

South Korea is particularly affected by its neighboring countries depending on the season, and the amount of fine dust is intensifying daily as a result of the traffic volume and industrial facilities in the cities. In accordance with such societal trends, the South Korean government provides information on fine dust to its citizens based on data collected from 323 Air Quality Monitoring Systems (AQMS) installed across the country. Fine dust is designated as PM10 and PM2.5, and the data about these particulates are provided in real time to citizens through a website and smartphone app. The AQMS, however, have significant installation and maintenance costs, and a lack of manpower for maintenance has resulted in a spatial imbalance in their installation. These devices are installed only in certain regions, and insufficiencies in the number of units make fine dust information monitoring difficult in wider regions. Determining the quantities and spatial distributions of fine dust is of the utmost importance for environmental improvement in urban areas and long-term policy implementation, but the delivery of accurate fine dust information to citizens is difficult due to the

 doi:10.20944/preprints201809.0280.v1

aforementioned issues. Research is being conducted on prediction of past spatial distributions of fine dust in order to resolve these issues.

Traditional methods of predicting spatial distributions of air quality, such as the amount of fine dust, include using the closest measurement data or the average values for an entire region [4, 5]. If one searches for air quality information about a certain place in Korea, the measurements from the closest AQMS are queried. However, high-resolution atmospheric pollutant distribution information is necessary to establish policies on urban planning, the environment, and health [6]. Various interpolation techniques such as kriging and inverse distance weighting (IDW) are being developed and utilized as spatial statistics methods to estimate values in locations that have not been measured. These methods are based on singular variables, but the distributions of atmospheric pollutants should be predicted using assorted variables according to the circumstances of the target areas because air quality is affected by complex processes, including climate, temperature, terrain, pollution source location, traffic volume, and land use [7].

Recently, studies have been conducted in which artificial intelligence (AI)-based artificial neural networks (ANNs) and machine learning were utilized by applying numerous variables to increase the prediction accuracy. Studies have also been conducted on Beijing, China, in which the universal kriging technique was employed to obtain fine dust distribution maps based on climate data and data collected by fine dust sensors [8]. In addition, atmospheric pollutant distribution prediction has been investigated by utilizing ANNs, land-use regression models, and machine learning techniques that account for factors that affect air quality distributions, such as those of fine dust [9–11].

The research methodologies for determining accurate air quality distributions are continually being elaborated upon because they are utilized not only for spatial decision-making, but also by individuals to make decisions regarding outdoor activities, which is especially critical for vulnerable groups, such as children and the elderly. There are also many people who want to have accurate fine dust information to make informed choices regarding outside activities or airing out their homes. With the continually increasing interest in fine dust, spatial analysis of the population that is exposed to fine dust is important.

An accurate survey of the population spread is first necessary to analyze the population that is exposed to fine dust. Population estimates are conducted using methods such as Bayesian models and random forests by downscaling population census data and analyzing the population spread [12, 13]. In these techniques, the population is calculated using a uniform spatial resolution of 100–1000 m units.

It is difficult to obtain accurate fine dust information for the residential districts of modern urban areas due to the insufficient number of AQMS devices and their uneven spatial distribution. Accordingly, the objective of the present study was to reduce the spatial imbalance of fine dust information that is provided to citizens. Specifically, land coverage, land use, emission source, and meteorological data were utilized to develop a particulate matter dispersion model and to construct fine dust concentration distribution maps. This report provides not only a comparison and analysis of the fine dust concentration distribution information available to citizens, but also quantitative analysis of the population that is exposed to fine dust based on elaborate population distribution data.

2. Materials and Methods

In the present study, Particulate matter dispersion modeling was utilized to examine the spatial errors of the fine dust information that citizens currently receive. The overarching research methodology employed was particulate matter dispersion modeling and geographic information systems (GISs) to generate fine dust concentration maps and to analyze the exposed population. The differences between the model developed in this research and the existing methodology were also examined by comparing the fine dust concentrations and populations exposed to fine dust according to the two methods. The overall methodology is illustrated in Figure 1.

Preprints (www.preprints.org) | NOT PEER-REVIEWED | Posted: 16 September 2018 doi:10.20944/preprints201809.0280.v1

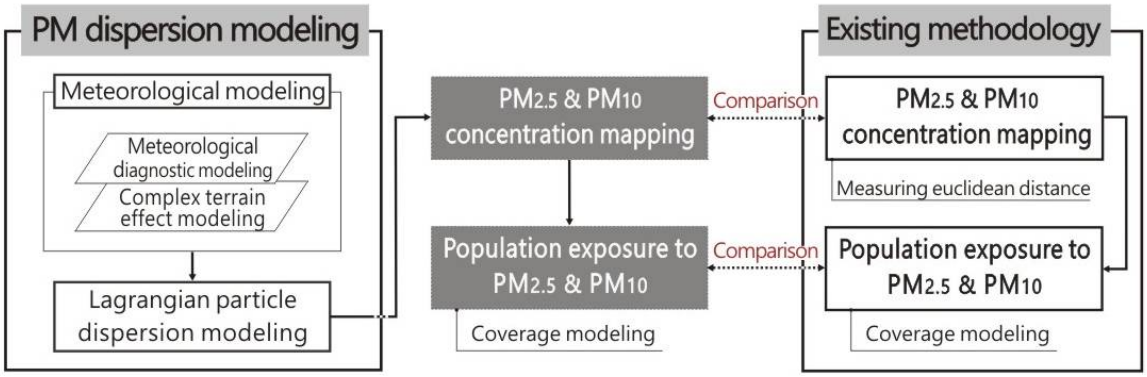

Figure 1. Diagram of overall research methodology.

2.1 Study Site

The study site was Daejeon Metropolitan City, which is located in the central region of South Korea. Daejeon is a large city with a high population density. As one of the five largest metropolitan cities in South Korea, Daejeon has an area of approximately 530 km², with a population of roughly 1.5 million people. Particulate matter dispersion modeling was conducted in a 6 km × 6 km area that included the area surrounding the city hall where the population is concentrated (Figure 2).

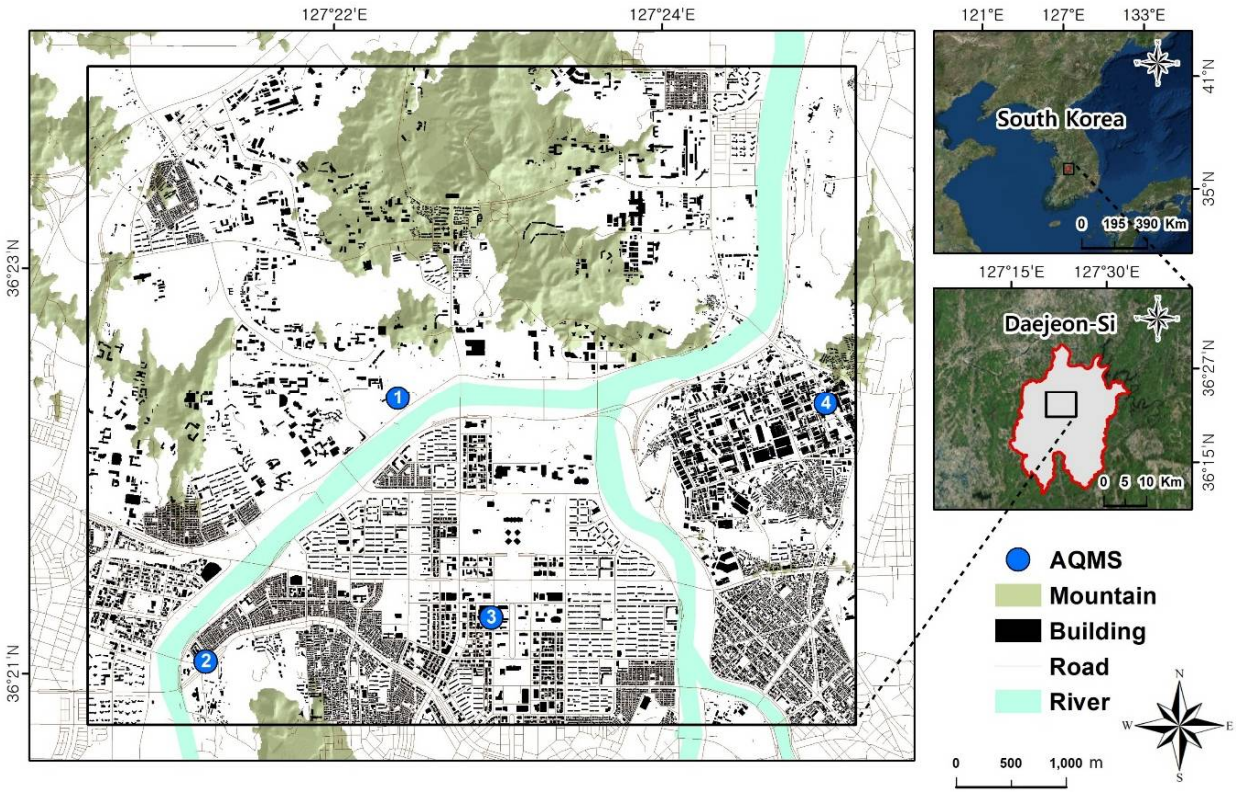

Figure 2. Study site.

The study site was divided into grids with a minimum size of 50 m, which includes the scale at which the dispersion and movement of atmospheric pollutants in the city can be examined. Each grid was analyzed to deduce its fine dust concentration.

2.2 Particulate Matter Dispersion Modeling

There are two main types of particulate matter dispersion models: meteorological models and Lagrangian particle dispersion models. The overall particulate matter dispersion modeling process used in this study is shown in Figure 3. The computer programming language Fortran 2003, which is primarily utilized in scientific numerical analysis, was employed.

Preprints (www.preprints.org) | NOT PEER-REVIEWED | Posted: 16 September 2018 doi:10.20944/preprints201809.0280.v1

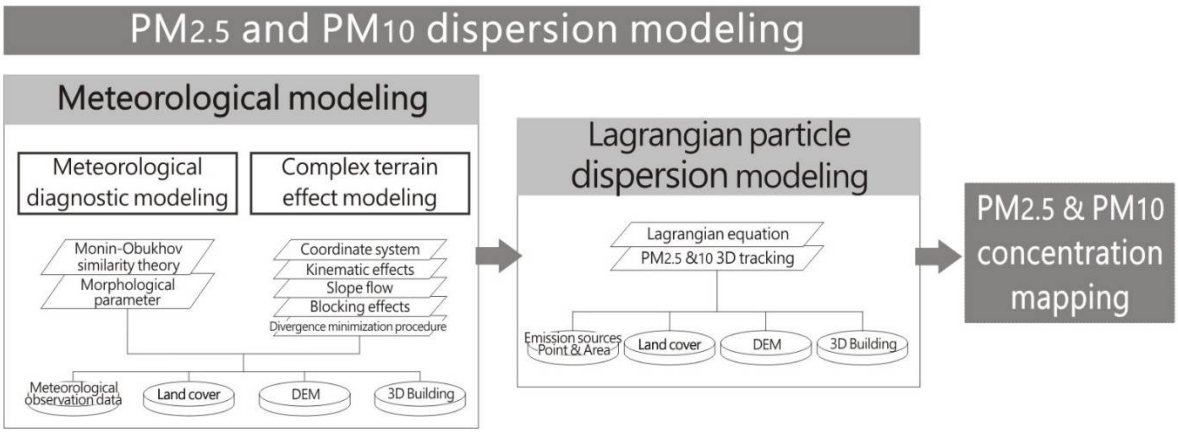

Figure 3. Particulate matter dispersion modeling process.

In meteorological modeling, meteorological observation dates, land coverage, digital elevation models (DEMs), and 3D buildings are used as input data. Meanwhile, in Lagrangian particle dispersion modeling, land coverage, DEMs, 3D buildings, and emission sources (points and areas) are used as input data. These inputs are summarized in Table 1 below.

Table 1. Input data for particulate matter dispersion modeling.

Model		Input data	Description
Particulate matter dispersion modeling	Meteorological model	Meteorological observation data	Weather station information that is either included in the target site or can influence the target site
		Land coverage	Conversion of land coverage information about the target site into 50 m grid units
		DEM	Conversion of terrain information about the target site into 50 m grid units
		3D building	3D information about the buildings included in the target site
	Lagrangian particle dispersion model	Emission sources (point)	Hourly quantity of atmospheric pollutant emission from smokestacks of emitting industries (330 smokestacks)
		Emission sources (area)	Conversion of information regarding traffic volume and emission pollutants at the target site into road emission source information
		Land coverage	Conversion of land coverage information about the target site into 50 m grid units
		DEM	Conversion of terrain information about the target site into 50 m grid units
		3D building	3D information about the buildings included in the target site

2.2.1 Meteorological Modeling

In meteorological models, weather observations are used to generate detailed wind fields and meteorological fields of target sites, and as diagnostic rather than prognostic models. Meteorological models produce meteorological information that is identical to the weather observations at any point in time [14].

Preprints (www.preprints.org) | NOT PEER-REVIEWED | Posted: 16 September 2018 doi:10.20944/preprints201809.0280.v1

Because nearly 65% of South Korea is comprised of mountainous areas, terrain must be considered, as there are also considerable terrain fluctuations in its cities. In addition, 3D meteorological field modeling should be conducted that takes into account buildings and various structures because South Korea has diverse infrastructure and a concentrated population. In meteorological modeling, a primary meteorological field is generated that accounts for flat areas, buildings, and structures through meteorological diagnostic modeling, and a final meteorological field is generated by producing a secondary meteorological field through complex terrain modeling that accounts for substantial terrain changes, such as those in mountainous regions.

In atmospheric boundary layer modeling in flat regions, meteorological observations and forecasts based on Monin–Obukhov similarity theory are utilized to generate meteorological information about the atmospheric boundary layer. The vertical distribution ($u(z)$) of the average wind velocity is given by Equation (1):

$$u(\mathrm{z}) = \frac{u^*}{k}\left[\ln\left(\frac{z}{L}\right) - \Psi_m\left(\frac{z}{L}\right) + \Psi_m\left(\frac{z_0}{L}\right)\right]. \quad (1)$$

Here, k is the von Kármán constant, u^* is the friction velocity, z is the vertical elevation calculated from the surface, z_0 is the surface roughness, L is the Monin–Obukhov length, and Ψ_m is a function that reflects atmospheric stability.

The form of Ψ_m depends on L, and a functional formula presented previously was applied in this study [14–16]. u^* and L are meteorological variables, but they must be calculated based on meteorological observations because they are not physical quantities measured at weather observation stations. L can be calculated using the following equation:

$$L = -\frac{pc_pT_{ref}u^{*3}}{kgH}. \quad (2)$$

Here, p is the air density, c_p is the specific heat at constant pressure, T_{ref} is the observation temperature, u^* is the friction velocity, k is the von Kármán constant, g is the gravitational acceleration (9.8 m/s^2), and H is the sensible heat flux.

H was obtained by employing an empirical formula presented previously [14, 17]. As shown in Equation (2), u^* and L are connected to one another, and because the value of just one of these quantities cannot be calculated sequentially, an iterative scheme must be used to obtain the values of both. In the iterative scheme described by Equation (1), Ψ_m is initially set to 0, and elevation and wind speed observations are employed to calculate u^*. The obtained value of u^* is then used in Equation (2) to calculate L, and hence to estimate Ψ_m. Next, the resulting value of Ψ_m is substituted into Equation (1) to recalculate u^*, and the result is again substituted into Equation (2) to calculate L. This process was repeated in this study for iterative calculation of u^* and L, and the deduced values of u^* and L were compared. The calculations agreed to within the margin of error.

Although urban areas are flat, their characteristically dense buildings and man-made structures affect the air currents. Morphological parameters have been used to estimate airflow distributions considering buildings and man-made structures [14, 18–21]. Urban spaces were divided into 100 m × 100 m grid units to calculate the statistics of the building shapes for each unit, and spaces with heights of 100 m from the ground were set as the morphological model domains.

The primary meteorological field was generated through meteorological diagnostic modeling in the target sites, where flat areas, buildings, and structures were accounted for through the above processes.

Complex terrain effect modeling was conducted to generate a secondary meteorological field. Urban areas with significant mountainous terrain can be affected considerably by the terrain. The terrain particularly affects the meteorological field adjacent to the ground surface. To account for the complexities of the terrain in this study, the meteorological fields were calculated taking into account five types of terrain effects, including coordinate system variations, kinematic effects, slope flow, blocking effects, and divergence minimization procedures in the equation for deducing the meteorological fields in flat areas.

For the grid system, the following equation was employed to generate a terrain-following vertical coordinate system:

Preprints (www.preprints.org) | NOT PEER-REVIEWED | Posted: 16 September 2018 doi:10.20944/preprints201809.0280.v1

$$X = x,\ Y = y,\ Z = z_p - h_T. \quad (3)$$

Here, x and y are the horizontal coordinates, Z is the vertical coordinate, z_p is the rectangular coordinate, and h_T is the altitude of the topography above sea level. In the vertical coordinate system, the vertical wind speed (w) can be calculated by employing the following equation:

$$w = w_p - u\frac{\partial h_T}{\partial x} - v\frac{\partial h_T}{\partial y}. \quad (4)$$

Here, w_p is the vertical wind speed (m/s) in the vertical coordinate system, and u and v are the east–west and north–south horizontal components (m/s) of the wind speed vector.

Kinematic effects reflect the tendency for airflow to form based on terrain, and w was calculated using the following modified equation [22]:

$$w = \left(\vec{V} \cdot \nabla h_T\right) \exp(-kz). \quad (5)$$

Here, $\vec{V}$ is the horizontal wind speed vector (u, v), and k is the vertical attenuation constant, which changes based on the atmospheric stability.

The slope flow can be calculated using the following equation based on the airflow that occurs due to differences in density along slopes [23]:

$$S = S_e[1 - exp(-x/L_e)]^{1/2}. \quad (6)$$

Here, S is the slope flow, S_e is the slope flow that reaches an equilibrium state, x is the distance from a valley to a slope, and L_e is the length to the arrival of an equilibrium state. S_e and L_e can be calculated by applying the following equations:

$$s_e = [hg(\Delta\theta/\theta)\sin\alpha/(C_d + k)\ ]^{1/2} \quad (7)$$

$$L_e = h/(C_D + k). \quad (8)$$

Here, h is the depth of the slope flow, g is the gravitational acceleration, $\Delta\theta$ is the potential temperature loss that occurs due to surface cooling, α is the elevation angle of a horizontal slope, C_D is the frictional force drag coefficient of the ground, and k is the model coefficient of the highest point of a gradient current.

Blocking effects occur when the atmospheric layer is stratified in a stable form due to the surface cooling effect, and airflow rotates on the peripherals rather than passing over the projecting terrain. The effects of blocked flow in a given direction due to the terrain are reflected by the Froude number [24], which can be calculated using the following equation:

$$F_r = \frac{V}{N\Delta h_T}. \quad (9)$$

Here, F_r is the local Froude number, V is the grid wind speed (m/s), N is the Brunt–Vis frequency (1/s), and Δh_T is the effective height (m) of the protruding terrain.

Lastly, the divergence minimization procedure must be considered. The divergence of the wind field where the terrain effect is reflected must be kept close to 0. The divergence at each grid point can be calculated using Equation (10):

$$D_{ijk} = \frac{w_{i,j,k+1/2} - w_{i,j,k-1/2}}{z_{k+1/2} - z_{k-1/2}} + \frac{u_{i+1,j,k} - u_{i-1,j,k}}{2\Delta x} + \frac{u_{i,j+1,k} - u_{i,j-1,k}}{2\Delta y}. \quad (10)$$

Here, D_{ijk} is the divergence (1/s) of grid point (i, j, k), and Δx and Δy are the grid intervals (m) in the x and y directions, respectively. The secondary meteorological field was generated through complex terrain effect modeling in areas that account for complex terrain, such as mountainous terrain, by employing the processes described above.

The primary and secondary meteorological fields were used to generate the final meteorological field, as shown in Equation (11):

$$u = \omega\, u_1 + (1 - \omega)u_2$$

$$v = \omega\, v_1 + (1 - \omega)v_2$$

$$w = \omega\, w_1 + (1 - \omega)w_2. \quad (11)$$

Preprints (www.preprints.org) | NOT PEER-REVIEWED | Posted: 16 September 2018 doi:10.20944/preprints201809.0280.v1

Here u, v, and w are the east and west components, the north and south components, and the vertical components of the wind respectively. u_1, v_1, and w_1 are the airflows of the primary meteorological field considering flat terrain, buildings, and structures; u_2, v_2, and w_2 are the airflows of the secondary meteorological field above complex terrain; and ω is a weight function variable established based on the number and elevation of the weather observation station; it has a real value between 0 and 1. If the complex terrain effect is marginal, as in ¤u_1 ≅¤ u_2, ¤v_1 ≅¤ v_2, and ¤w_1 ≅¤ w_2, the first meteorological field may be viewed as the final meteorological field.

2.2.2 Lagrangian Particle Dispersion Modeling

Lagrangian particle dispersion models are popular tools for simulating the dispersion of trace gases, aerosols, or radionuclides in the atmosphere [25–29]. These models are primarily utilized as atmospheric diffusion models and as sophisticated models for calculating changes in wind direction. Due to topographic characteristics and chemical changes in pollutants based on time, they can trace the migration of air masses [14]. In Lagrangian particle dispersion modeling, particle movements during a time dt (s) can be expressed as Langevin equations [30]:

$$du = -\frac{u}{T_{Lu}}dt + \sqrt{C_0\epsilon dt}\omega_u$$

$$dv = -\frac{v}{T_{Lv}}dt + \sqrt{C_0\epsilon dt}\omega_v$$

$$dw = -\frac{w}{T_{Lw}}dt + \sqrt{C_0\epsilon dt}\omega_w. \quad (12)$$

Here, T_{Lu}, T_{Lv}, and T_{Lw} are the Langrangian time scales of the x, y, and z directions, respectively, which can be defined as in Equation (13):

$$T_{Lu} = 2\frac{{\sigma^2}_u}{C_{0\epsilon}}$$

$$T_{Lv} = 2\frac{{\sigma^2}_v}{C_{0\epsilon}}$$

$$T_{Lw} = 2\frac{{\sigma^2}_w}{C_{0\epsilon}}. \quad (13)$$

Here, ${\sigma^2}_u$, ${\sigma^2}_v$, and ${\sigma^2}_w$ are the turbulent energies (m^2/s^2) in the x, y, and z directions, respectively.

2.2.3 Particulate Matter Dispersion Modeling Verification and Mapping

To verify the modeling, the work conducted by Raupach and Legg [31], which is widely quoted in literature related to atmospheric diffusion in the field of fluid dynamics, was employed in this study. Raupach and Legg [31] designed a sophisticated wind tunnel experiment and performed a thermal diffusion experiment. In the present study, the variables and environment used in the wind tunnel experiment were implemented, and the particulate matter dispersion modeling was verified by comparing the data obtained in this study with those of Raupach and Legg [31].

The movement and dispersion of fine dust change continually based on the wind direction, wind speed, weather conditions, and natural or artificial environments. Thus, fine dust concentrations can be visualized in 1 h intervals based on weather observations. The PM2.5 and PM10 concentration standards are divided by each of their concentrations. The concentration of PM2.5 is designated as "Good" when it is 0–15 μg/m³, "Moderate" when it is 16–35 μg/m³, "Unhealthy" when it is 36–75 μg/m³, and "Very Unhealthy" when it is over 76 μg/m³, while that of PM10 is designated as "Good" when it is 0–30 μg/m³, "Moderate" when it is 31–80 μg/m³, "Unhealthy" when it is 81–150 μg/m³, and "Very Unhealthy" when it is over 151 μg/m³. These are the fine dust concentration standards currently provided to citizens and are similar to those advised by developed nations and the World Health Organization (WHO).

264

265 *2.3 Comparison with Existing Methodology and Analysis*

266 2.3.1 Comparison and Analysis of Fine Dust Concentration Maps

267 As mentioned previously, the fine dust concentrations that are currently provided to citizens by
268 the state provide concentrations measured in real time at AQMS in 1 h intervals. Queries for
269 concentrations can be done via the internet or a smartphone to obtain the concentrations from the
270 AQMS closest to the current location of the user. The closest fine dust concentrations can be
271 determined using the Euclidean distance measurement method. In this study, the fine dust
272 concentration maps deduced through Euclidean distance measurement were compared with those
273 deduced using the particulate matter dispersion model developed in this study, and the differences
274 were analyzed. GIS ArcMap 10.3 was used for the Euclidean distance measurements.

275 2.3.2 Comparison and Analysis of Population Exposed to Fine Dust

276 The exposed population was calculated, compared, and analyzed based on fine dust maps
277 constructed using the existing methodology and particulate matter dispersion modeling. Census data
278 were employed to determine the exposed population. The census data included the population
279 residing in buildings and were provided by the state as populations within 100 m × 100 m areas.
280 Downscaling these data, the population was calculated within 50 m × 50 m units for the target site in
281 this study. A coverage model [32, 33] was employed for the population calculations within the
282 concentration map, using the following equation:

283 $$\text{Coverage} = \sum_p S_p. \quad (14)$$

284 Here, S_p is the distribution area by fine dust concentration, and p is the population.

Preprints (www.preprints.org) | NOT PEER-REVIEWED | Posted: 16 September 2018 doi:10.20944/preprints201809.0280.v1

3. Results

3.1 Particulate Matter Dispersion Modeling Verification and Mapping

In the simulations conducted in the present research, the variables were implemented to model an environment such as that used by Raupach and Legg [31], and the results of their wind tunnel experiment were compared with those obtained using the model developed in this study. Figure 4(a) depicts the data from the wind tunnel experiment conducted by Raupach and Legg [31], which are overlapped with the results of this study in Figure 4(b).

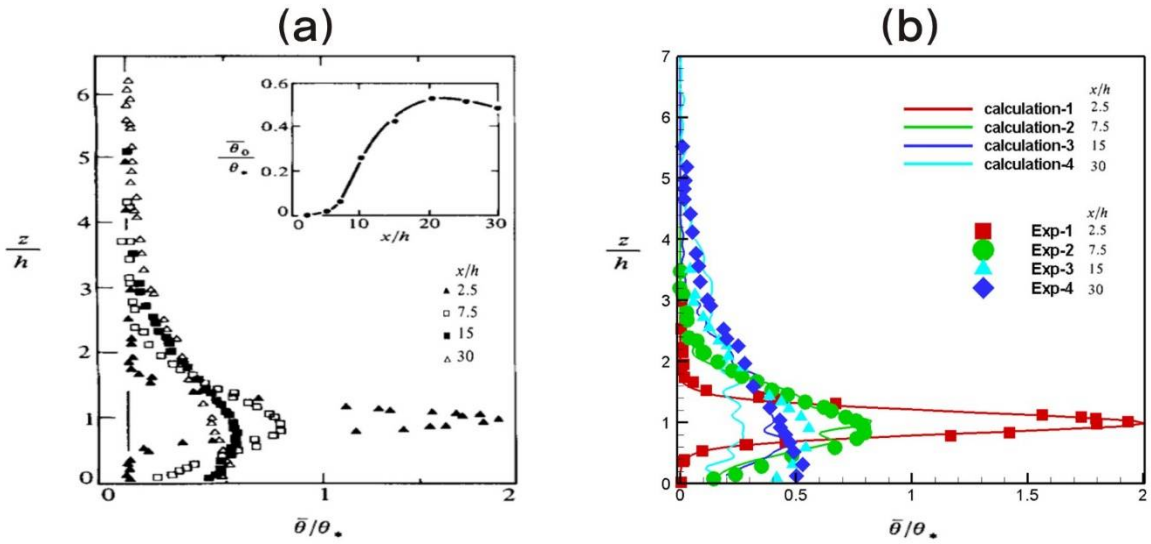

Figure 4. (a) Data from the wind tunnel experiment conducted by Raupach and Legg [31], and (b) overlapping of the data from this study with that obtained by Raupach and Legg [31]. $\boldsymbol{x/h}$ is the distance from the source point, $\boldsymbol{h}$ is the height of the source emissions, $\overline{\boldsymbol{\theta_0}}$ is the air temperature relative to the ambient air temperature, and $\boldsymbol{\theta_*}$ is the temperature scale. The calculations of Raupach and Legg [31] are designated as "Exp," and those obtained using the model developed in this study are designated as "calculation."

The experimental results obtained in four environments (a–d) were compared based on the distance from the source point, and R^2 was used to analyze the relationships between the data obtained in this study and those of Raupach and Legg [31] (Figure 5).

Preprints (www.preprints.org) | NOT PEER-REVIEWED | Posted: 16 September 2018 doi:10.20944/preprints201809.0280.v1

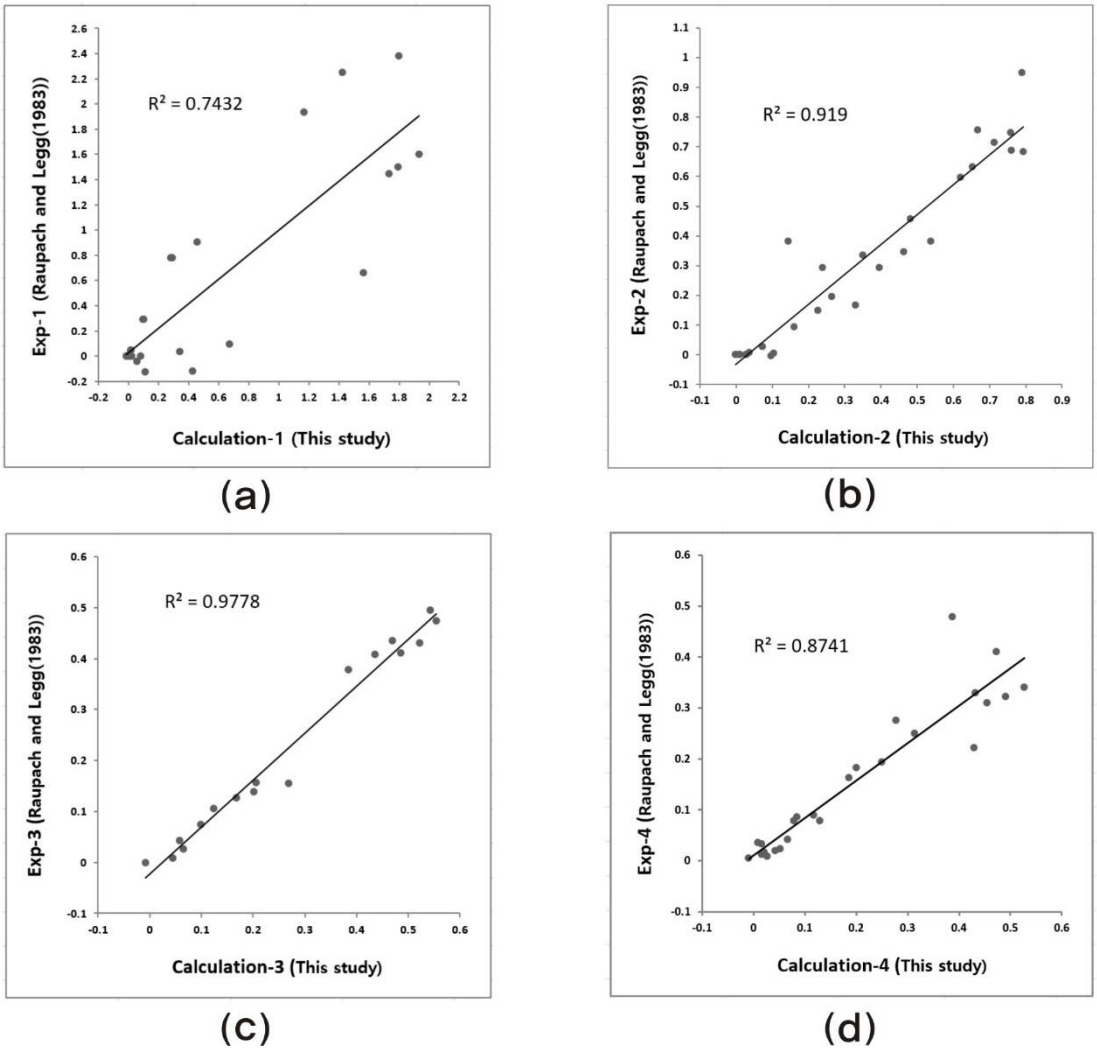

Figure 4. Correlation analysis of the results obtained in the preceding research with those of the present study. (a)–(d) Comparison of the experimental results obtained in four environments based on distance from the source point.

The R^2 values in environments (b) and (c) demonstrate exceptionally high explanatory power above 0.9. Environments (a) and (d) also exhibit high explanatory powers, above 0.7 and 0.8, respectively, demonstrating that the model developed in this study provides results similar to those obtained in the preceding research.

Fine dust concentration maps based on input data from 1 h intervals can be constructed in 1 h intervals in particulate matter dispersion modeling. In this study, concentration maps were created based on a large amount of fine dust data, and the relationships between the results from particulate matter dispersion modeling and the data from AQMS was observed. Figure 6 depicts the PM2.5 concentration maps obtained via dispersion modeling in the areas surrounding AQMS units.

Preprints (www.preprints.org) | NOT PEER-REVIEWED | Posted: 16 September 2018 doi:10.20944/preprints201809.0280.v1

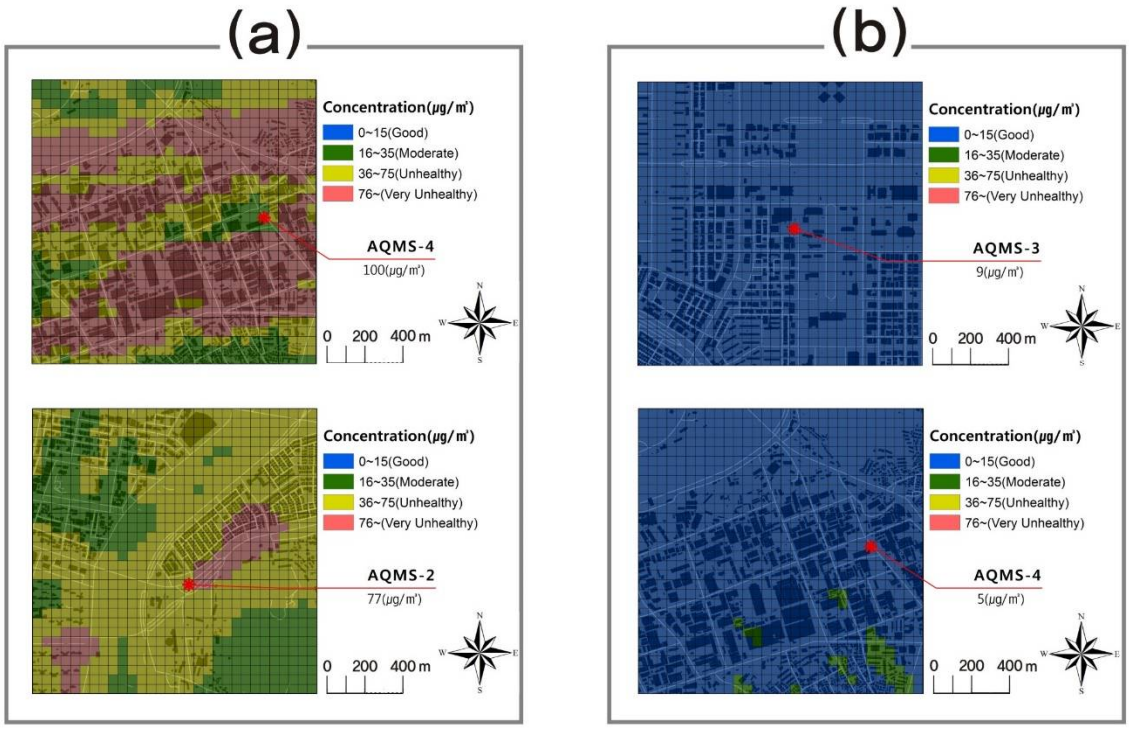

Figure 5. PM2.5 dispersion modeling results. Days with (a) poor and (b) favorable amounts of fine dust according to the AQMS values.

Figures 6(a) and (b) present the PM2.5 dispersion modeling concentration maps for one day. Figure 6(a) shows that the fine dust concentration is generally poor, while Figure 6(b) shows that the fine dust concentration is generally good. Similar concentrations can be found by comparing the measured concentrations of AQMS.

Figure 7 presents the PM10 dispersion modeling results obtained in expanded areas surrounding the AQMS.

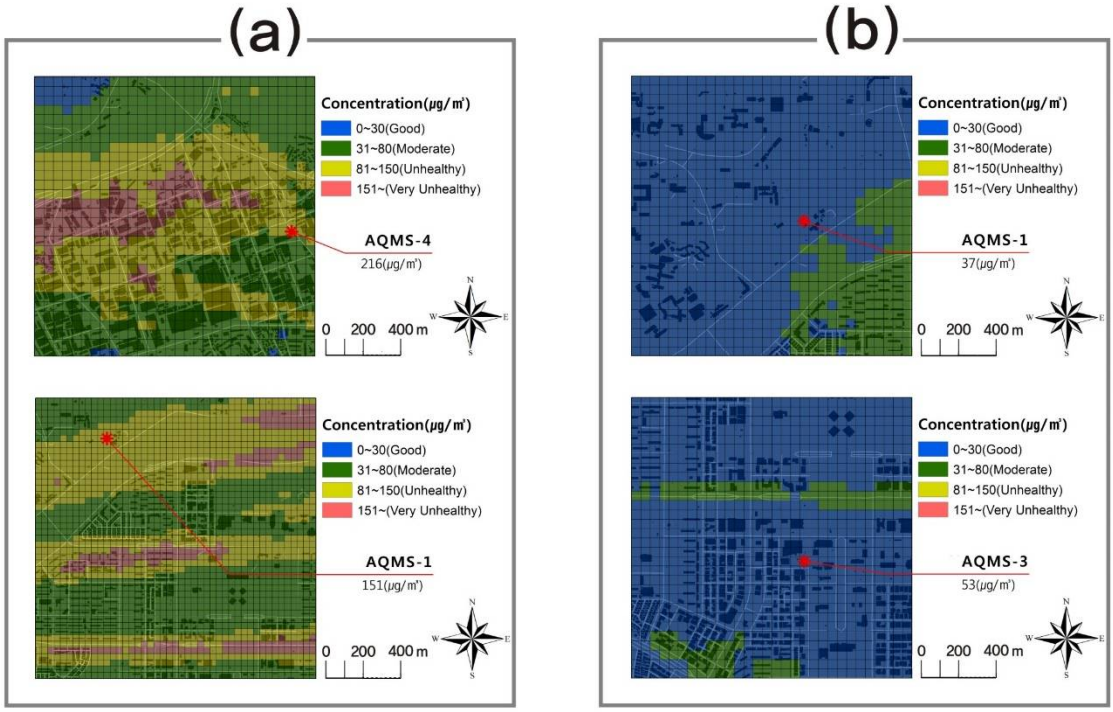

Preprints (www.preprints.org) | NOT PEER-REVIEWED | Posted: 16 September 2018 doi:10.20944/preprints201809.0280.v1

Figure 6. PM10 dispersion modeling results. (a) Days with poor fine dust values and (b) days with favorable fine dust values in the AQMS values.

Figures 7(a) and (b) present the PM10 dispersion modeling concentration maps for one day. Figure 7(a) shows that the fine dust concentration is generally poor, while Figure 7(b) shows that the fine dust concentration is generally good. Similar concentrations can be found by comparing the measured concentrations of AQMS.

Although the fine dust patterns constructed through modeling are similar to the AQMS values, they differ when examining only the cells in which AQMS units are installed. This issue will be addressed in section 4.

3.2 Comparison and Analysis of Existing Methodology

3.2.1 Comparison and Analysis of Fine Dust Concentration Maps

The fine dust information that is provided to citizens is received from the AQMS closest to the query location. This existing methodology was employed to generate concentration maps using GIS Euclidean distance measurements. The maps for the four investigated areas were constructed by Euclidean distance measurement with the four AQMS devices in the target sites as starting points.

The concentration maps created through particulate matter dispersion modeling according to the method developed in this study were generated based on the fine dust concentrations of over 16,000 cells, where each concentration was calculated within a 50 m × 50 m cell of the target site.

Figure 8 presents sample PM2.5 concentration maps created using the existing methodology and PM2.5 dispersion modeling. In Map 1, 2, and 3 of Figure 8, differences can be seen between the maps generated using the two techniques. According to the existing methodology, the PM2.5 concentrations are "Good" or "Moderate," while those obtained via dispersion modeling are frequently "Unhealthy" or "Very Unhealthy." These differences could mean that the PM2.5 concentration information provided to citizens is inaccurate. In map 4 of Figure 8, the results of the existing methodology and PM2.5 dispersion modeling are similar. While some of the modeling values are designated as "Unhealthy," they comprise a relatively insignificant portion of the overall map.

Preprints (www.preprints.org) | NOT PEER-REVIEWED | Posted: 16 September 2018 doi:10.20944/preprints201809.0280.v1

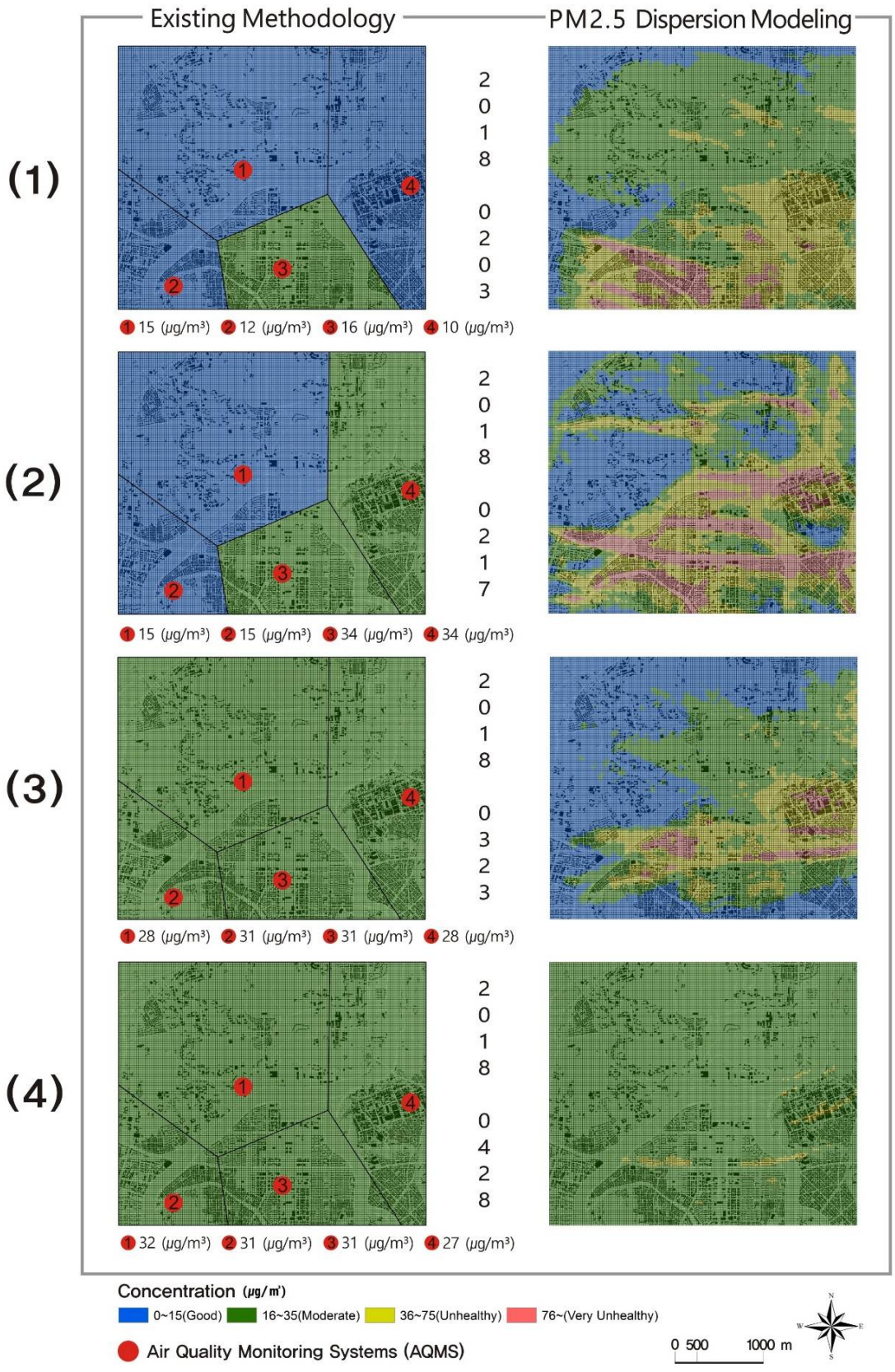

Figure 7. Comparison of PM2.5 concentration maps constructed using the existing methodology and PM2.5 dispersion modeling.

Table 2 provides a comparison of the results obtained using the existing methodology and PM2.5 dispersion modeling as ratios.

Preprints (www.preprints.org) | NOT PEER-REVIEWED | Posted: 16 September 2018 doi:10.20944/preprints201809.0280.v1

Table 2. Comparison of concentration ratios according to the existing methodology and PM2.5 dispersion modeling.

Concentration (μg/m³)	Existing Methodology (%)				PM2.5 Dispersion Modeling (%)			
	(1) 20180203	(2) 20180217	(3) 20180323	(4) 20180428	(1) 20180203	(2) 20180217	(3) 20180323	(4) 20180428
Good (0–15)	82.72024	56.30357	0	0	16.25	31.35714	46.66667	0
Moderate (16–35)	17.27976	43.69643	100	100	52.19048	25.85714	33.20238	98.27976
Unhealthy (36–75)	0	0	0	0	26.06548	27.76786	16.64286	1.720238
Very Unhealthy (>76)	0	0	0	0	5.494048	15.01786	3.488095	0

In case 1 of Table 2, the differences between the concentrations obtained using the existing methodology and PM2.5 dispersion modeling can be seen quantitatively in Table 2. According to the existing methodology, the concentration is "Good," meaning that most people can engage in outdoor activities safely in more than 80% of the area. However, according to the modeling results, more than 30% of the concentrations are bad, and "Moderate" concentrations exist in more than 50% of the areas. The fine dust standards of WHO and developed nations state that "Moderate" concentrations can have adverse effects on vulnerable populations, such as children and the elderly. Aside from case 4 of Table 2, there are significant differences between the values obtained using the two methodologies according to Table 2.

Figure 9 presents PM10 concentration maps created using the existing methodology and particulate matter dispersion modeling. Map 1 of Figure 9 exhibits "Moderate" fine dust concentrations everywhere, but the modeling results display "Good," "Moderate," "Unhealthy," and "Very Unhealthy" concentrations. Map 2 of Figure 9 only shows the areas near AQMS-3 as being "Unhealthy" and the other areas as "Moderate," while the modeling results show "Good," "Moderate," "Unhealthy," and "Very Unhealthy" concentrations. Map 3 of Figure 9 differs from the others. According to the existing methodology, the areas near AQMS-1 have "Unhealthy" concentrations, but the modeling results show "Good" or "Moderate" concentrations. Finally, map 4 of Figure 9 indicates that the fine dust concentration is generally "Moderate," but also exhibits extensive regions with "Very Unhealthy" concentrations.

Preprints (www.preprints.org) | NOT PEER-REVIEWED | Posted: 16 September 2018 doi:10.20944/preprints201809.0280.v1

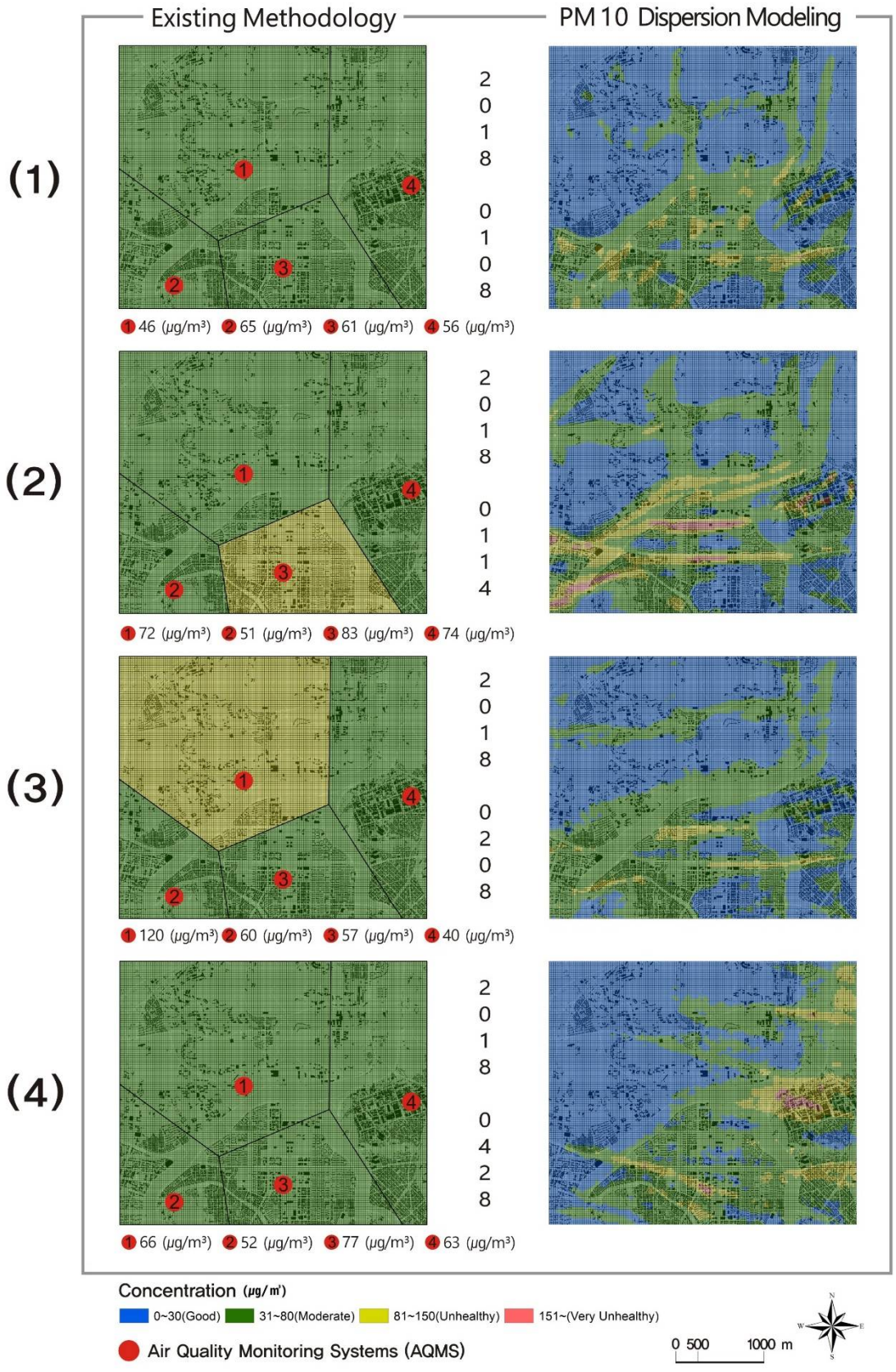

Figure 8. Comparison of PM10 concentration maps constructed using the existing methodology and PM10 dispersion modeling.

Table 3 provides a comparison of the concentration results obtained using the existing methodology and PM10 dispersion modeling as ratios.

Preprints (www.preprints.org) | NOT PEER-REVIEWED | Posted: 16 September 2018 doi:10.20944/preprints201809.0280.v1

Table 3. Comparison of concentration ratios obtained using the existing methodology and PM10 dispersion modeling.

Concentration (μg/m³)	Existing Methodology (%)				PM10 dispersion modeling (%)			
	(1) 20180108	(2) 20180114	(3) 20180208	(4) 20180428	(1) 20180108	(2) 20180114	(3) 20180208	(4) 20180428
Good (0–30)	0	0	0	0	58.67857	47.38095	54.54762	48.66071
Moderate (31–80)	100	82.72024	56.89881	100	36.65476	40.64286	43.09524	41.875
Unhealthy (81–150)	0	17.27976	43.10119	0	4.642857	10.08929	2.357143	8.77381
Very Unhealthy (>151)	0	0	0	0	0.02381	1.886905	0	0.690476

In case 1 of Table 3, all of the concentrations are "Moderate," according to the existing methodology, but the modeling results show all of the concentration levels. The results for case 2 indicate that approximately 2% of the sections have "Very Unhealthy" concentrations, but these regions constitute an area of roughly 800,000 m², the majority of which is residential. The spatial interpretation will be addressed in greater detail in section 4. In case 3 of Table 3, the "Unhealthy" areas comprise approximately 43% according to the existing methodology, indicating restrictions on outdoor activities and ventilation, but these areas constitute only about 2% in the modeling results. In case 4 of Table 3, the overall target site is at a "Moderate" level according to the existing methodology, but the modeling results show PM10 concentrations at "Unhealthy" and "Very Unhealthy" levels in approximately 10% of the target site. Thus, an area of approximately 4,000,000 m², which was concentrated around residential areas, had high PM10 concentrations.

3.2.2 Comparison and Analysis of Population Exposed to Fine Dust

The populations exposed to PM2.5 according to the existing methodology and PM2.5 dispersion modeling were also compared. Figure 10 depicts the areas where people live on the PM2.5 concentration maps constructed using the existing methodology and PM2.5 dispersion modeling. In map 1, all of the people are exposed to "Moderate" concentrations, according to the existing methodology, but based on the modeling results, approximately 100,000 people are exposed to "Unhealthy" and "Very Unhealthy" concentrations. In map 2, approximately 100,000 people are exposed to "Good" concentrations, according to the existing methodology, but the modeling results show that over 170,000 people are exposed to "Unhealthy" and "Very Unhealthy" levels.

Preprints (www.preprints.org) | NOT PEER-REVIEWED | Posted: 16 September 2018 doi:10.20944/preprints201809.0280.v1

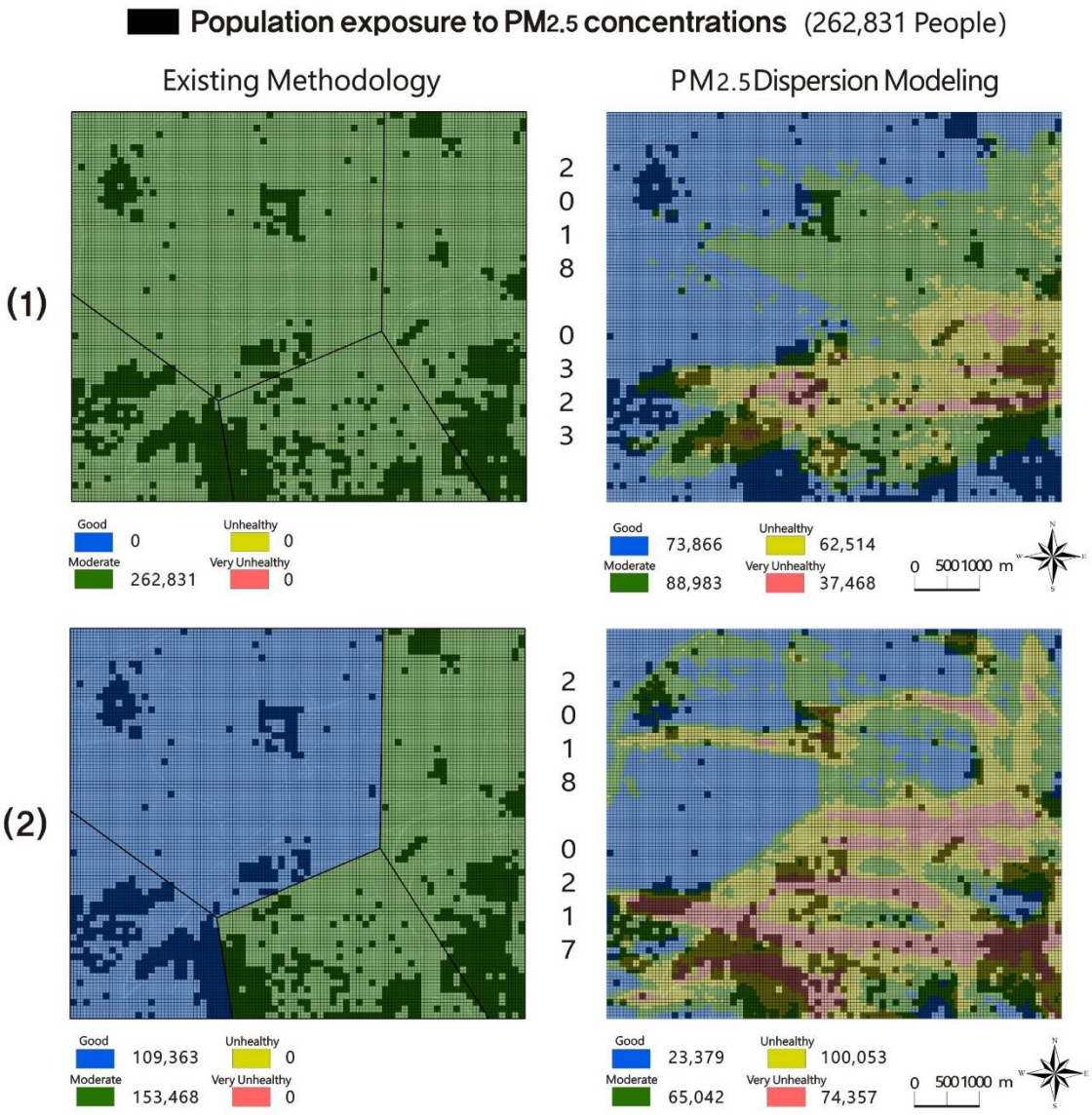

Figure 9. Comparison of populations exposed to different PM2.5 concentrations, according to the existing methodology and PM2.5 dispersion modeling.

Similarly, the populations exposed to PM10 according to the existing methodology and dispersion modeling were compared. Figure 11 depicts the areas where people live on the PM10 concentration maps constructed using the existing methodology and dispersion modeling. In map 1, no one is exposed to "Good" or "Very Unhealthy" concentrations, according to the existing methodology, but the modeling results show that more than 70,000 people are exposed to "Good" levels and more than 10,000 are exposed to "Very Unhealthy" levels. In map 2, all of the population is exposed to "Moderate" concentrations, according to the existing methodology, but the modeling results show that the population is exposed to all concentration levels.

Preprints (www.preprints.org) | NOT PEER-REVIEWED | Posted: 16 September 2018 doi:10.20944/preprints201809.0280.v1

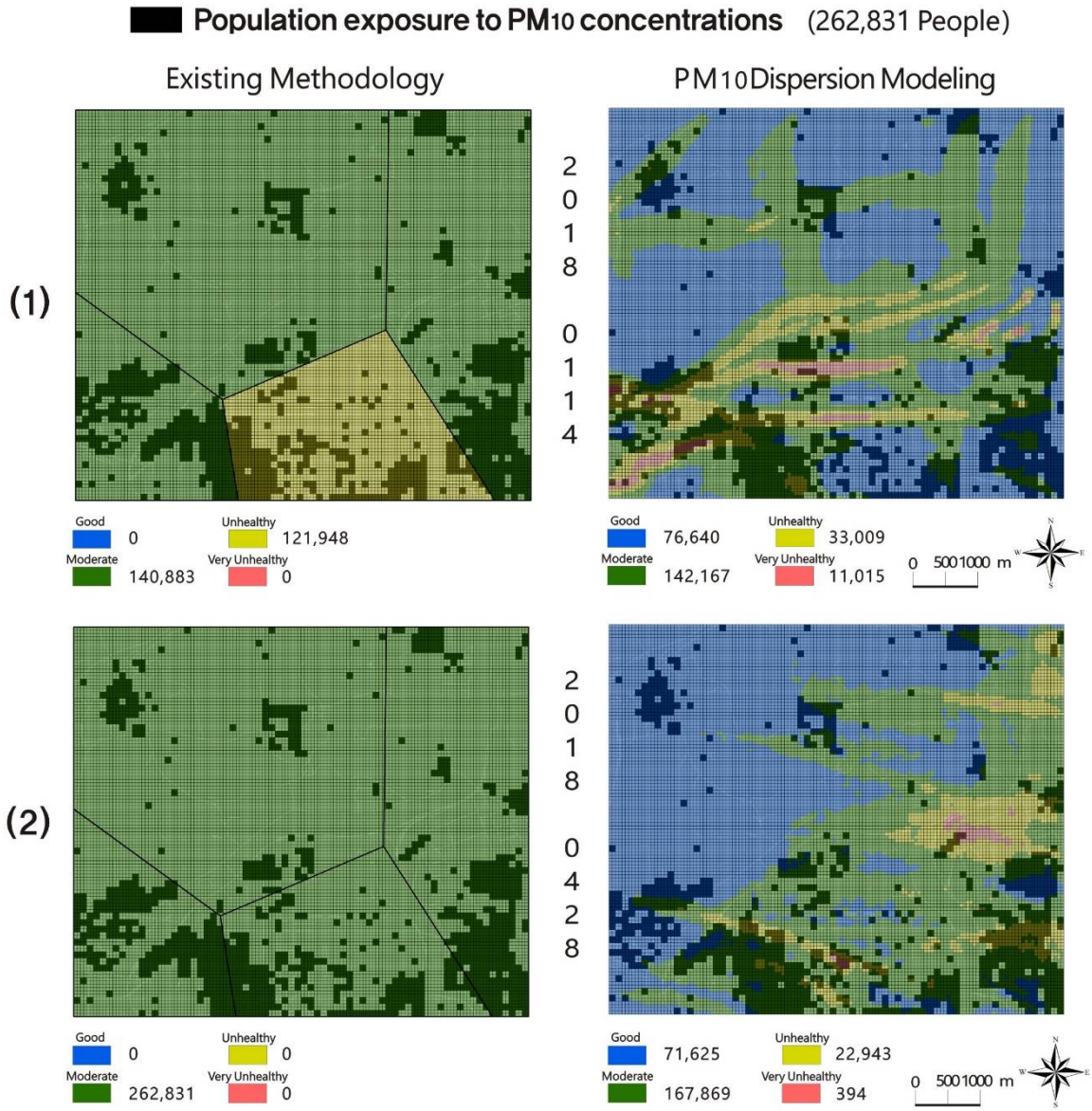

Figure 101. Comparison of populations exposed to various PM10 concentrations, according to the existing methodology and PM10 dispersion modeling.

4. Discussion

4.1 Particulate Matter Dispersion Modeling

In the particulate matter dispersion model developed in the present study, the meteorological and Lagrangian particle dispersion models are utilized to determine the dispersion of fine dust in urban areas. Differences were observed between the fine dust concentration maps created using this model and those currently provided to citizens. As mentioned above, fine dust information is acquired from the nearest AQMS. However, Rodriguez et al. [7] stated that the distribution of atmospheric pollutants must be predicted by taking into account numerous variables, including land use, pollution source location, traffic volume, and temperature. Thus, the particulate matter dispersion model that considers these variables is more precise than the existing methodology.

There are various techniques for fine dust distribution prediction, but that currently used to provide information to citizens is a very simple one based on Euclidean distance measurement. In this method, spaces are simply divided according to the distances measured between AQMS units,

Preprints (www.preprints.org) | NOT PEER-REVIEWED | Posted: 16 September 2018 doi:10.20944/preprints201809.0280.v1

without regard to any other variables. The fine dust maps obtained using the existing methodology in Figures 8 and 9 depict the fine dust concentrations in four areas, and each can only be verified with identical numerical values. In addition, Tables 2 and 3 show that, according to the existing methodology, there are almost no "Unhealthy" and "Very Unhealthy" concentrations, which differs from the results obtained by modeling. The kriging method [8] is more precise than the existing methodology (Euclidean distance measurement), and can be used to forecast the air quality of an entire target site. Although this methodology has higher predictive accuracy with a higher number of real measurement values, some AQMS devices were installed in the target sites in this study, and thus, fine dust measurements could have been inaccurate if the above method had been employed. Kriging and IDW are spatial statistics methods based on GIS, but these methods would not have been able to reflect the characteristics of the target sites in this study, such as land use or emission source.

Recently, high-dimensional data analysis methodologies have also been employed. Kleine Deters et al. [11] utilized meteorological and pollutant data obtained over the previous 6 years and forecasted future fine dust concentrations via machine learning methods. This methodology differs from that employed in the present study as it involves the use of numerous data points observed in the past to forecast the future. The methodology utilized in this study enables current concentrations or those 1 h later to be determined using meteorological data that is provided in 1 h intervals. Unlike in the study conducted by Deters et al. [11], it was possible to extract accurate fine dust concentrations through modeling that minutely reflected the characteristics of the investigated areas in the present study. Future research that merges the modeling employed in this study with machine learning or AI methods to deduce fine dust concentrations could be meaningful.

The Lagrangian particle dispersion model used in the particulate matter dispersion model that was developed in this study is a 3D numerical analysis model that is primarily utilized with the Eulerian model when modeling atmospheric dispersion. However, it has the disadvantage that its results are difficult to compare with measurements from air pollution monitoring stations. In addition, the modeling results shown in Figures 6 and 7 indicate that there are differences between the AQMS fine dust concentrations and modeling values in identical cells. The reason for this discrepancy appears to be the complexity of the algorithm that includes the dispersion and movement of fine dust based on wind direction and speed, as well as land use and emission source.

4.2 Spatial Distribution of Fine Dust and Exposed Populations

The results of the particulate matter dispersion model developed in this study revealed high fine dust concentrations mainly in the southern and eastern areas, where a river was flowing horizontally through the center of the region. The target site had a mountainous area to the north whose parts remained mostly urbanized. The complex terrain was reflected in the developed particulate matter dispersion model to calculate the meteorological field. As such, even if the fine dust concentration was high in the south, the effects of wind blowing in the mountainous areas in the north resulted in low fine dust concentrations. AQMS-1, which is located in the north, also yielded mostly lower concentrations than the AQMS located in the remaining three areas.

According to existing research methodologies, the AQMS data at one location represent the entirety of the corresponding area, while the modeling results provide fine dust concentrations by cell. The modeling results in Figure 8 reveal high PM2.5 concentrations in the south and east where there is a high density of buildings. The reason for this finding can be approached from a variety of perspectives. First, industrial complexes, which are the leading source of pollution, are located in the east, where there is also a developed road network with a significant volume of traffic. Studies in which fine dust concentrations due to vehicles have been measured on the sides of roads based on elevation [34, 35] have indicated that high fine dust concentrations occur at low elevations due to vehicles. It is also necessary to consider high fine dust concentration values that occur due to buildings. High-rise apartments and other buildings are located in areas with high concentrations, and 3D building and structural information was also utilized in the developed particulate matter dispersion model. Although they did not address buildings, Liu et al. [36] performed fine dust concentration measurements by elevation along roads lined with tall trees on both sides. Their results

indicated that there were higher fine dust concentrations than in the surrounding areas. It is possible that high buildings impact wind paths similarly, causing fine dust to stagnate between buildings.

In addition to spatial fine dust concentration analysis, it is also necessary to analyze exposed populations, which is important for urban and environmental planning. A small portion of the population may be exposed in areas where poor fine dust concentrations are widely distributed, and a large portion of the people in densely populated areas may be exposed even if poor fine dust concentrations are narrowly distributed. For instance, the PM2.5 concentrations on February 17, 2018, in Figures 8 and 10 show that while approximately 40% of the target area had poor PM2.5 levels, around 70% of the entire population was exposed to those levels. Similarly, the PM10 concentrations on January 14, 2018, in Figures 9 and 11 reveal that while only 10% of the target area had poor PM10 concentrations, over 40,000 people were exposed to those concentrations.

To achieve cities that are free from fine dust, the creation of sustainable cities and environmental planning based on the above results that account for land use and exposed populations is necessary, as well as the use of green spaces and proper wind paths and continuous environmental monitoring of emission sources.

5. Conclusions

The present study was conducted with an awareness of the errors in the fine dust concentrations currently provided to citizens. Motivated by this awareness, the fine dust concentrations obtained using the existing methodology and dispersion modeling were compared with each other and analyzed. The exposed populations according to these two methodologies were also examined. While the fine dust concentrations currently available are simply representative values provided by AQMS, those obtained by modeling account for the present conditions of the target site and meteorological factors. Thus, the results yielded by the two methodologies differed from each other. Modeling was able to provide the detailed spatial distributions of fine dust concentrations and exposed populations. As the harm caused by fine dust is becoming more severe worldwide, this research will contribute to sustainable urban and environmental planning.

Since the emission information used in the particulate matter dispersion model developed in this study was survey data rather than real-time observations, future studies should be conducted using real-time observations. In addition, when exposed populations are calculated in future studies, smartphone data should be employed, and the exposed population should be calculated by taking into account current location rather than place of residence.

Above all, to provide fine dust concentrations, such as those deduced in this study, through smartphones or websites in real time, research and technical skills related to data connections, algorithm loading, and communications are needed from an information systems perspective, and systems and policies that can contribute to sustainable urban environments should be considered.

Author Contributions: The first author, Seungwoo Son, developed the flow of this study, wrote most of manuscript, and performed the dispersion modeling. Hyungjin Jeon, Dongwoo Kim, and Jaejin Yu wrote some of the manuscript and conducted a GIS analysis. Seogcheol Kim and Kyunghak Cho performed the particle matter dispersion modeling. Youngeun Kang reviewed the manuscript and contributed to the research design.

Acknowledgments: This study was funded by the Korea Environmental Industry & Technology Institute (KEITI) under grant [number: 2016000200009] and conducted by the Korea Environment Institute (KEI).

Conflicts of Interest: The authors declare no conflict of interest.

References

1. World Health Organization. *Ambient Air pollution: A Global Assessment of Exposure and Burden of Disease.* World Health Organization, Geneva, Switzerland, 2016, ISBN: 9789241511353.
2. Guerreiro, C.B.; Foltescu, V.; De Leeuw, F. Air quality status and trends in Europe. *Atmos. Environ.* **2014**, *98*, 376-384.

3. Schneider, P.; Castell, N.; Vogt, M.; Dauge, F.R.; Lahoz, W.A.; Bartonova, A. Mapping urban air quality in near real-time using observations from low-cost sensors and model information. *Environ. Int.* **2017**, *106*, 234-247.
4. Pope III, C.A.; Dockery, D.W. Health effects of fine particulate air pollution: lines that connect. *J. Air Waste Manag. Assoc.* **2006**, *56*(6), 709-742.
5. Yanosky, J.D.; Paciorek, C.J.; Laden, F.; Hart, J.E.; Puett, R.C.; Liao, D.; Suh, H.H. Spatio-temporal modeling of particulate air pollution in the conterminous United States using geographic and meteorological predictors. *Environ. Health* **2014**, *13*(1), 63.
6. Beelen, R.; Hoek, G.; Pebesma, E.; Vienneau, D.; de Hoogh, K.; Briggs, D.J. Mapping of background air pollution at a fine spatial scale across the European Union. *Sci. Total Environ.* **2009**, *407*(6), 1852-1867.
7. Rodríguez, M.C.; Dupont-Courtade, L.; Oueslati, W. Air pollution and urban structure linkages: Evidence from European cities. *Renew. Sustain. Energ. Rev.* **2016**, *53*, 1-9.
8. Liu, Z.; Xie, M.; Tian, K.; Gao, P. GIS-based analysis of population exposure to PM2. 5 air pollution—A case study of Beijing. *J. Environ. Sci.* **2017**, *59*, 48-53.
9. Zheng, Y.; Liu, F.; Hsieh, H.P. U-Air: When urban air quality inference meets big data. In Proceedings of the 19th ACM SIGKDD International Conference on Knowledge Discovery and Data Mining. ACM: Chicago, IL, 2013, pp. 1436-1444.
10. Deville Cavellin, L.; Weichenthal, S.; Tack, R.; Ragettli, M.S.; Smargiassi, A.; Hatzopoulou, M. Investigating the use of portable air pollution sensors to capture the spatial variability of traffic-related air pollution. *Environ. Sci. Technol.* **2015**, *50*(1), 313-320.
11. Kleine Deters, J.; Zalakeviciute, R.; Gonzalez, M.; Rybarczyk, Y. Modeling PM2.5 urban pollution using machine learning and selected meteorological parameters. *J. Electr. Comput. Eng.* **2017**, *2017*, 5106045.
12. Alegana, V.A.; Atkinson, P.M.; Pezzulo, C.; Sorichetta, A.; Weiss, D.; Bird, T.; Erbach-Schoenberg, E.; Tatem, A.J. Fine resolution mapping of population age-structures for health and development applications. *J. Royal Soc. Interface* **2015**, *12*(105), 20150073.
13. Stevens, F.R.; Gaughan, A.E.; Linard, C.; Tatem, A.J. Disaggregating census data for population mapping using random forests with remotely-sensed and ancillary data. *PloS One* **2015**, *10*(2), e0107042.
14. Kim, S.C.; Lee, J.S.; Yun, J.I.; Kang, J.H.; Kim, W.S. Study on Lagrangian heat source tracking method for urban thermal environment simulations. *J. Korean Soc. Atmos. Environ.* **2017**, *33*(6), 583-592.
15. Panofsky, H.A.; Dutton, J.A. *Atmospheric Turbulence: Models and Methods for Engineering Applications*, Wiley: New York, NY, USA, 1984, p. 397, ISBN: 9780471057147.
16. Van Ulden, A.P.; Holtslag, A.A.M. Estimation of atmospheric boundary layer parameters for diffusion applications. *J. Clim. Appl. Meteorol.* **1985**, *24*(11), 1196-1207.
17. De Bruin, H.A.R.; Holtslag, A.A.M. A simple parameterization of the surface fluxes of sensible and latent heat during daytime compared with the Penman-Monteith concept. *J. Appl. Meteorol.* **1982**, *21*(11), 1610-1621.
18. Macdonald, R.W.; Griffiths, R.F.; Hall, D.J. An improved method for the estimation of surface roughness of obstacle arrays. *Atmos. Environ.* **1998**, *32*(11), 1857-1864.
19. Macdonald, R. W. Modelling the mean velocity profile in the urban canopy layer. *Boundary Layer Meteorol.* **2000**, *97*(1), 25-45.
20. Bentham, T.; Britter, R. Spatially averaged flow within obstacle arrays. *Atmos. Environ.* **2003**, *37*(15), 2037-2043.
21. Hanna, S.R.; Britter, R.E. *Wind Flow and Vapor Cloud Dispersion at Industrial and Urban Sites*, John Wiley & Sons: Hoboken, NJ, USA, 2010; Volume 7, ISBN: 9780816908639.
22. Liu, M.K.; Yocke, M.A. Siting of wind turbine generators in complex terrain. *J. Energ.* **1980**, *4*(1), 10-16.
23. Mahrt, L. Momentum balance of gravity flows. *J. Atmos. Sci.* **1982**, *39*(12), 2701-2711.
24. Allwine, K.J.; Whiteman, C.D. *MELSAR: A Mesoscale Air Quality Model for Complex Terrain. Overview, Technical Description and User's Guide (No. PNL-5460-Vol. 1)*. Pacific Northwest Labs, Richland, WA, USA, 1985; Volume 1.
25. Stohl, A.; Klimont, Z.; Eckhardt, S.; Kupiainen, K.; Shevchenko, V.P.; Kopeikin, V.M.; Novigatsky, A.N. Black carbon in the Arctic: the underestimated role of gas flaring and residential combustion emissions. *Atmos. Chem. Phys.* **2013**, *13*(17), 8833-8855.
26. Lin, J.C.; Gerbig, C.; Wofsy, S.C.; Andrews, A.E.; Daube, B.C.; Davis, K.J.; Grainger, C.A. A near-field tool for simulating the upstream influence of atmospheric observations: The stochastic time-inverted Lagrangian transport (STILT) model. *J. Geophys. Res. Atmos.* **2003**, *108*(D16).

27. Witham, C.S.; Hort, M.C.; Potts, R.; Servranckx, R.; Husson, P.; Bonnardot, F. Comparison of VAAC atmospheric dispersion models using the 1 November 2004 Grimsvötn eruption. *Meteorol. Appl.* **2007**, *14*(1), 27-38.
28. Stein, A.F.; Draxler, R.R.; Rolph, G.D.; Stunder, B.J.; Cohen, M.D.; Ngan, F. NOAA's HYSPLIT atmospheric transport and dispersion modeling system. *Bull. Am. Meteorol. Soc*. **2015**, *96*(12), 2059-2077.
29. Eckhardt, S.; Cassiani, M.; Evangeliou, N.; Sollum, E.; Pisso, I.; Stohl, A. Source–receptor matrix calculation for deposited mass with the Lagrangian particle dispersion model FLEXPART v10. 2 in backward mode. *Geosci. Model Dev.*, **2017**, *10*, 4605-4618.
30. Borgas, M.S.; Sawford, B.L. A family of stochastic models for two-particle dispersion in isotropic homogeneous stationary turbulence. *J. Fluid Mech.* **1994**, *279*, 69-99.
31. Raupach, M.R.; Legg, B.J. Turbulent dispersion from an elevated line source: measurements of wind-concentration moments and budgets. *J. Fluid Mech*. **1983**, *136*, 111-137.
32. Talen, E. Neighborhoods as service providers: a methodology for evaluating pedestrian access. *Environ. Plan. B* **2003**, *30*(2), 181-200.
33. Son, S.W.; Ahn, T.M. Sensitivity analysis on the population within and outside of the Urban Park Service areas - Focused on Daegu Metropolitan City neighborhood parks and resident registration number data. *J. Korean Inst. Landscape Archit*. **2013**, *41*(5), 9-18.
34. Weber, K.; Heweling, G.; Fischer, C.; Lange, M. The use of an octocopter UAV for the determination of air pollutants–a case study of the traffic induced pollution plume around a river bridge in Duesseldorf, Germany. *Int. J. Environ. Sci.* **2017**, *2*, 63-68.
35. Villa, T.F.; Jayaratne, E.R.; Gonzalez, L.F.; Morawska, L. Determination of the vertical profile of particle number concentration adjacent to a motorway using an unmanned aerial vehicle. *Environ. Pollut.* **2017**, *230*, 134-142.
36. Liu, F.; Zheng, X.; Qian, H. Comparison of particle concentration vertical profiles between downtown and urban forest park in Nanjing (China). *Atmos. Pollut. Res*. **2018**, *9*(5), 829-839.